Cleaner technology for the production of linear long chain α-olefins through a "millisecond" oxidative cracking process

Hugo Cruchade, Claude Veit, Jean-Jacques Colin, Romain Beauchet, Yann Batonneau, Yannick Pouilloux, Bertrand Leroux, Ludovic Pinard

▶ **To cite this version:**

Hugo Cruchade, Claude Veit, Jean-Jacques Colin, Romain Beauchet, Yann Batonneau, et al.. Cleaner technology for the production of linear long chain α-olefins through a "millisecond" oxidative cracking process. Applied Catalysis A : General, 2021, 610, pp.117944 -. ⟨10.1016/j.apcata.2020.117944⟩. ⟨hal-03493332⟩

HAL Id: hal-03493332

https://hal.science/hal-03493332v1

Submitted on 2 Jan 2023

HAL is a multi-disciplinary open access archive for the deposit and dissemination of scientific research documents, whether they are published or not. The documents may come from teaching and research institutions in France or abroad, or from public or private research centers.

L'archive ouverte pluridisciplinaire **HAL**, est destinée au dépôt et à la diffusion de documents scientifiques de niveau recherche, publiés ou non, émanant des établissements d'enseignement et de recherche français ou étrangers, des laboratoires publics ou privés.

Distributed under a Creative Commons CC BY-NC 4.0 - Attribution - Non-commercial use - International License

Version of Record: https://www.sciencedirect.com/science/article/pii/S0926860X20305378
Manuscript_60b86f370dc9d2fde162b28c5494e8d9

Cleaner technology for the production of linear long chain α-olefins through a "millisecond" oxidative cracking process.

Hugo Cruchade, Claude Veit, Jean-Jacques Colin, Romain Beauchet, Yann Batonneau, Yannick Pouilloux, Bertrand Leroux, Ludovic Pinard*

Institut de Chimie des Milieux et Matériaux de Poitiers (IC2MP), UMR 7285 CNRS, 4 rue Michel Brunet, Bâtiment B27, TSA 51106, 86073 Poitiers Cedex 9 – France.

*Corresponding author ludovic.pinard@univ-poitiers.fr

Abstract

The oxidative cracking of *n*-decane was investigated at millisecond contact times over platinum alumina washcoated monoliths at a fuel-air equivalent ratio (Φ) of 5. High valuable linear α-olefins were so produced through an autothermal way concomitantly with oxygenated compounds, CO, CO_2, H_2 and H_2O.

A fine identification of reaction products coupled with the study of thermal phenomena occurring with both active and deactivated catalysts allowed to investigate the *n*-decane transformation mechanism and to discriminate heterogeneous and homogeneous reactions. This process is a 2-zone reaction system involving catalytic combustion of one part of reactant which provides enough heat for gas phase radical transformations initiation. Long chain hydrocarbons result from homogeneous decomposition of oxygenated intermediates such as decylperoxy radicals into aldehydes and α-olefins.

Keywords: α–olefins, oxygenates, partial oxidation, homogeneous heterogeneous reactions.

© 2020 published by Elsevier. This manuscript is made available under the CC BY NC user license
https://creativecommons.org/licenses/by-nc/4.0/

1. Introduction

Linear α-olefins (LAO) are pervasive as raw materials for daily lives products such as plastics, packaging, detergents, paints and lubricants for mechanics engines [1]. Ethylene oligomerization provides the whole of LAO market [1,2] and operates with homogeneous catalysts in an organic solvent between 100 and 250 °C and under high pressures (> 100 atm) [1,3]. Most of LAO units use Ziegler and Ziegler-Natta type catalysts such as in Gulfene, Ethyl and Idemistsu processes. These processes are unselective and lead to a Schulz-Flory or Poisson type distribution of LAO chain lengths [3]. Contrariwise, Shell Higher Olefins Process (SHOP), which uses nickel coordination compounds, is versatile and able to adapt the selectivity to the market need thank to the double bond isomerization followed by the disproportionation of undesired LAO [4].

A cleaner technology to produce LAO could consist in the oxidative cracking (OC) of hydrocarbons on a heterogeneous catalyst in a millisecond reactor operating under atmospheric pressure. Schmidt *et al.* developed this technology primarily for the production of syngas from methane partial oxidation [5–9]; light olefins from ethane [5,10–13] and propane [10,11,14] oxidative dehydrogenation and C_4-C_8 hydrocarbons oxidative cracking [14–18]. In few works they demonstrate its relevance for LAO synthesis from higher *n*-alkanes (*n*-decane [19] and *n*-hexadecane [20,21]).

Partial oxidation of hydrocarbons into syngas is carried out on Rh catalysts and at fuel-air equivalent ratio (Φ) close to 3 [5,10,15,22,23], which is defined as the ratio of fuel-to-oxidizer ratio of the reaction to the stoichiometric fuel to oxidizer combustion ratio. This exothermal reaction imposes reactional temperatures above 1000 °C. On lean mixtures (Φ > 3), unreacted fuel cracks into olefins through endothermal reactions [17,21,24]. The required heat is then provided by exothermal oxidation reactions, allowing to reach an autothermal state of the process. Combustion catalysts such as platinum are then preferable to produce

olefins [19,25]. It is well established than millisecond reactors are 2-zone reaction systems [17,25–28] , implying heat generation from catalytic combustion of a part of the reactant and gas phase formation of olefins from unreacted fuels. While light alkanes homogeneous oxidative dehydrogenation into corresponding alkenes occurs through radical oxygen-assisted or pyrolytic mechanism [25,29–31] within the channels and downstream of the monolith [13,32,33], the path of LAOs formation from higher *n*-alkanes is yet unclear. These products are obtained at catalyst equilibrium temperatures below 800 °C, resulting into yields of 60 % from *n*-decane [19] and *n*-hexadecane [21] oxidative cracking. Considering the incomplete oxygen consumption from combustion reactions at these temperatures, the higher reactivity of long chain hydrocarbons for oxidation reactions [34] and lower C-C bond energy [35], the millisecond oxidative cracking of higher *n*-alkanes could involve different heterogeneous and homogeneous mechanisms.

The purpose of this study is to evaluate the performances of the millisecond oxidative cracking of a model molecule, *n*-decane, on a fresh and aged platinum-based catalyst at a fuel-air equivalent ratio $\Phi = 5$. The efficiency will be evaluated in terms of thermal balance and yield into α–olefins. The study of thermal phenomena occurring during the OC of a model molecule (*n*-decane) coupled with the identification of products (through gas chromatography-mass spectroscopy (GC-MS)) will be carried out in order to understand all the mechanisms involved. The two catalytic systems (fresh and aged catalysts) will allow to discriminate the heterogeneous and homogeneous transformations occurring in a millisecond reactor, while maintaining constant hydrodynamic operation and similar thermal behavior of gas phase.

2. Experimental

2.1. Catalyst preparation

Cordierite monoliths (CTI, 15.8 mm diameter, 5 mm length, 600 cells per square inch (cpsi) were washcoated with gamma-alumina from a procedure adapted from the work of Amariei *et al.* [36]. The preparation method consisted in dipping the monolith into a sol prepared by adding boehmite (Disperal P2, Sasol) into an acidified aqueous (0.3 mol L^{-1} HNO_3 in ultrapure water) urea (Sigma-Aldrich, 99%) solution. After unclogging of the channels and drying, monoliths were calcined at 500 °C. Washcoated monoliths were then immersed in an aqueous (ultrapure water) solution of platinum salt precursor ($H_2PtCl_6 \cdot 6H_2O$, Alfa Aesar). Impregnation step ended after complete evaporation of the solvent in a sand bath. Finally, after drying, they were calcined at 500 °C for 2 h and reduced at 800 °C for 2 h. Catalyst aging was carried out through ten cycles of long-time reaction (24 h) - regeneration at high temperature (> 800 °C). Chemical and structural properties of the catalytic material were characterized using Inductively Coupled Plasma-Optical Emission Spectrometry (ICP-OES, Agilent 5110), Transmission Electron Microscopy (TEM, JEOL 2100 UHR) and nitrogen sorptiometry (Micromeritics Tristar 2). Initial activities were evaluated for the reaction of propane dehydrogenation at 575 °C and at total gas flow rate of 0.1 NL min^{-1} (GHSV = 18300 h^{-1}) with a composition of $C_3H_8/N_2/H_2$ at a volumetric ratio of 50/45/5. Results are summarized in **Table 1**.

2.2. Catalytic test

The experimental setup, represented in **Figure 1**, is composed of three main parts consisting in a reactant feeding system, a reactor and an analytical device. They are detailed in subsections 2.2.1, 2.2.2 and 2.2.3, respectively.

2.2.1. Feeding device

The reactor was fed with air, provided by a mass flow controller (Bronkhorst) and purified by a moisture adsorber (Molecular sieve 13 X, Prolabo) followed by activated charcoal (Roth). Liquid *n*-decane (≥ 99 %, Sigma-Aldrich), contained in a 10 psi pressurized tank, was introduced by an automotive injector (E.F.S.) downstream of the tank. The periodical opening of automotive injector allowed to pulverize pressurized liquid on the reactor walls.

2.2.2. Reactor

The reactor consisted of a quartz tube (16 mm inner diameter (ID), 755 mm length), inserted in two tubular ovens. A first tubular oven (260 mm length) was used to preheat the reactants, to vaporize *n*-decane and to mix it homogeneously with air. A second tubular oven (200 mm length) was used to provide the heat required for reactions. Temperature profiles were recorded using K-type thermocouples (1 mm diameter) inserted in a thermocouple well inside the reactor and positioned at 0, 10 and 55 mm downstream of the back face of the catalyst. Two reaction times were calculated from the two distinct areas of reaction (1) the contact time ($\tau_{Contact}$) of the reactants with the solid monolith, corresponding to heterogeneous area and (2) the residence time ($\tau_{Residence}$) of the reactants in the activation oven, corresponding to homogeneous area (**Figure 1**). Pressure was measured using a pressure gauge positioned at the reactor head.

2.2.3. Product Analysis

The gas flow at the reactor outlet was divided: (i) a portion is sent to an online gas chromatography (GC) and (ii) the main flow past through a condenser at 5 °C in order to sample liquid products for offline analysis. All the gas lines between the reactor outlet and the online GC were heated by heating tapes to avoid any condensation.

2.2.3.1. Products quantification online by internal standard

The products were quantified online with a SCION 456 gas chromatography, outlined in supporting information (**Figure SI. 1**) and equipped with three detectors: (1) a Thermal Conductivity Detector (TCD) fitted with a Hayesep Q (0.25 m × 1/16 in. outer diameter (OD), 1 mm ID, 80-100 mesh) packed column followed by a Molsieve 13X (0.25 m × 1/16 in. OD, 1 mm ID, 80-100 mesh) packed column for the analysis of H_2, O_2, N_2, CO_2, CO. (2) Two Flame Ionization Detectors (FID) fitted with a CP-Wax 58 CB (50 m × 0.32 mm, 0.5 µm film thickness) capillary precolumn followed by a Rt-Alumina/MAPD (30 m × 0.32 mm, 0.5 µm film thickness) capillary column for the analysis of C_1 to C_5 hydrocarbons and a SCION-1MS (30 m × 0.32 mm, 0.5 µm film thickness) capillary column for the analysis of higher hydrocarbons. Gas sampling was provided by heated Valco valves, allowing to inject repeatable quantities of gas. TCD were calibrated from gas mixtures of known pure compounds diluted in nitrogen. For FID calibrations, a known concentration of hydrocarbons gas mixture (alkanes and 1-alkenes) from C_1 to C_6 provided by Air Liquide was used to determine the carbon response coefficient. Response coefficients of oxygenated products were estimated using the Effective Carbon Number (ECN) concept [37] after offline identification through GC-MS.

2.2.3.2. Condensable products identification offline

In order to simplify the identification, the condensates were preliminary fractionated through two different technics (1) distillation at atmospheric pressure and (2) solid-phase extraction (SPE). The fractions were also injected in the online GC in order to correlate the retention times of identified compounds through GC-MS.

Solid-phase extraction: a silica cartridge (Bond Elut-SI, 1.5 g, 3 mL, 40 µm, Agilent) was washed with *n*-pentane (7 mL) before introducing the sample. The cartridge was then washed

with *n*-pentane (5 mL) and dried before elution with CH_2Cl_2 (5 mL) and finally with methanol (3 mL).

GC-MS analyses: The GC (Agilent 7890A)-MS (Agilent Accurate-mass QTOF 7200) device was fitted with a DB-Wax (40 m × 0.18 mm, 0.30 µm film thickness) capillary column followed by a SCION-1MS (30 m × 0.32 mm, 0.25 µm film thickness) capillary column.

2.2.4. Experimental procedure

At the startup of the process, the preheating and activation ovens are heated at the desired temperatures with a constant feeding of 2 NL min^{-1} of air. The reactor is then fed with 14 mg s^{-1} of *n*-decane and a temperature increase measured by K-type thermocouples is observed. After some minutes the temperature keeps constant, the process is operating at its steady state at a pressure close to 112 kPa. In the experiments conditions, $\tau_{Contact}$ and $\tau_{Residence}$ are close to 10 ms and to 0.5 s respectively (at average temperatures of 550 and 400 °C respectively). The online analysis is carried out at different time-on-stream. Typical chromatograms of the three channels are available in the supporting information (**Figure SI. 2**). From these chromatograms, conversions and yields are calculated as follows.

The molar flow of a compound *i* at the reactor outlet (F_i in mol min^{-1}), was determined from internal GC calibration with inert nitrogen:

$$F_i = K_i \times S_i \times \frac{F_{N_2}}{S_{N_2} \times K_{N_2}}.$$

Were S_i and S_{N_2} are the chromatograms peaks surfaces and K_i and K_{N_2} the response factors of species i and N_2 respectively.

Assuming the quantification of all outlet compounds, conversion of *n*-decane ($X_{n-decane}$) was determined as follows:

$$X_{n-decane} = \frac{\sum_i (x_i \times F_{i,products})}{\sum_i (x_i \times F_i)} \times 100.$$

Were x_i is the number of carbons atoms in the compound *i*.

Dioxygen conversion was calculated from inlet molar flow ($F_{O_2,0}$) provided by mass flow controller:

$$X_{O_2} = \frac{F_{O_2,0} - F_{O_2}}{F_{O_2,0}} \times 100.$$

The yield of hydrocarbon product *j* (Y_j) were reported on a carbon atom basis as follows:

$$Y_j = \frac{x_j \times F_j}{\sum_i (x_i \times F_i)} \times 100.$$

The hydrogen yield (Y_{H_2}) was reported on a hydrogen atom basis:

$$Y_{H_2} = \frac{y_j \times F_j}{\sum_i (y_i \times F_i)} \times 100.$$

Were y_j and y_i are the number of carbons atoms in the compounds *j* and *i* respectively.

Oxygen atom balance was closed to determine water molar flow rate and carbon and hydrogen atom balances were typically closed within ± 8 %, similar to Schmidt *et al.* [15,21].

The fuel-air equivalent ratio (Φ) refers to the following equation:

$$\phi = \frac{\frac{\sum_i (x_i \times F_i)}{F_{O_2,0}}}{\left(\frac{F_{C_{10}H_{22}}}{F_{O_2}}\right)_{Stoichiometry}}$$

3. Results and discussion

n-decane oxidative cracking is carried out with a fuel-air equivalent ratio (Φ) of 5 on a fresh and aged Pt/Al_2O_3 catalysts. The catalysts are in the shape of monolith with cells per square inch of 600. **Table 1** summarizes the main physicochemical properties of the catalysts.

Cordierite monoliths have a specific surface area close to zero which is dramatically augmented through washcoating of porous gamma-alumina. The aged catalyst, obtained after ten reaction-regeneration cycles at high temperature lost more than two thirds of its initial surface area, which indicates a washcoat morphology degradation. Fresh catalysts have similar Pt nanoparticles properties as regards of average diameter (1.4-1.5 nm), dispersion (77-81%) (**Table 1**) and size distribution (**Figure SI. 3** and **Figure SI. 4.A** respectively). After aging, Pt particles sintered (**Figure SI. 4.B** and **C**), leading to a bimodal distribution with larger particles (average diameters of 11.1 nm) and a lower dispersion (10 %) **Table 1**. Aged catalyst disclosed an initial activity for propane dehydrogenation reaction a half that of the fresh catalyst (**Table 1**), confirming the decrease of dispersion.

Figure 2 compares temperature profiles measured at different points downstream of the reactor with and without reaction on the fresh and aged catalysts.

Prior to gas feeding, the catalyst is preheated at 400 °C. In order to characterize the thermal loss during the gas release, experiment was merely carried out under air flow. After the shutdown of the oven, it immediately cools and whatever the point of temperature measurement, they decrease exponentially. These evolutions can be characterized by the thermal time constant (τ, **Table SI. 1**).

Upon flowing *n*-decane through the automotive injector, temperature of the monolith rises up to 600 °C on the fresh catalyst then rapidly decreases to reach a plateau at 550 °C. Therefore the process operates autothermally. Part of the heat released by reactions compensates for the thermal losses of the oven. There is a significant temperature gradient downstream of the monolith as the temperature falls down to 230 °C at 55 mm. The thermal time constant is twice as much as the one obtained without reaction (**Table SI. 1**). This strong thermal gradient can quench some combustion reactions. When nitrogen replaces feed gases, temperatures suddenly drop (τ) and the process spontaneously extinguishes.

On aged catalyst, the temperature profile is different, with lower temperatures (-100 to -350 °C), no stationary state, moreover the process extinguishes from 400°C even without stop the feed gas. It is worth noting that at 55 mm from the back-face monolith, the temperature remains constant for 10 min after catalyst extinction which could indicate that exothermic reactions still to occur during the extinction. After switching from reacting gas to air, an exotherm appears on the monolith back face, probably due to the coke combustion.

Without catalyst and under same conditions (*i.e.* blank test), no stationary state is observed, only the cooling of gas phase.

n-decane oxidative cracking yields CO_2, CO, oxygenated compounds, decenes, α-olefins, light olefins, methane and hydrogen as well as water (not quantified). The yields into carbonaceous products and oxygen conversion are shown at different reaction times on fresh and aged catalysts and during the blank test in **Figure 3**. Hydrogen yield on fresh and aged catalysts are shown in **Figure 4** at different reaction times. No carbon formation is observed on the reactor walls and no traces of coupled and aromatic products are detected. Their formation requires a longer residence time at high temperature (0.1 s to 1 s) as in the steam cracking [38].

Without catalyst, the reactor cooling extinguishes homogeneous reactions, oxygen and *n*-decane conversions reach respectively 4 % and 3 % at a gas phase temperature of 220 °C (**Figure 3**). Low activity catalyst is then required to sustain a temperature high enough to initiate homogeneous reactions.

On fresh catalyst, more than 93 % of oxygen is consumed throughout the run, while the conversion into *n*-decane is incomplete and decreases with time-on-stream (TOS). Yet, it remains high even after 1 and 3 h (*ca* 50 %, **Figure 3**). The incomplete conversion of oxygen is due to the very short contact time throughout the monolith (τ = 10 ms).

The yield into hydrogen, initially important, diminishes with the TOS (**Figure 4**), while remaining much more important than on aged catalyst. This suggests that hydrogen is produced catalytically during the combustion probably by the water-gas shift reaction (WGSR): $CO + H_2O \rightleftharpoons CO_2 + H_2$. or steam reforming: $C_xH_{2x} + xH_2O \rightleftharpoons xCO + 2xH_2$. WGSR is thermodynamically favored at low temperature, yet it is kinetically favored at high temperature. Indeed, several authors have shown that catalytic combustion dominates in the first millimeter of the catalyst bed [13,17,27,29,39,40], H_2 and CO being mostly produced along with some H_2O and CO_2. Moreover the temperature is 100-200 °C higher than the one measured at the catalytic bed outlet.

The decrease of CO and CO_2 yields leads automatically to the loss of heat generation, resulting in a temperature decrease and therefore a loss of catalyst activity. The deactivation also impacts selectivities. Olefins selectivity decreases concomitantly with an increase in oxygenated products.

On aged catalyst, the oxygen conversion is lower than that on the fresh one and decreases with the time-on-stream. The conversion of *n*-decane is similar to that of the stabilized fresh catalyst despite the temperature drop of the monolith (-250°C). On the other hand, selectivities are different with more oxygenated products. All of them are produced through homogeneous reactions that occur downstream of the monolith [16,41–43]. So, on fresh catalyst, both heterogeneous and homogeneous reactions occur simultaneously while on the aged one (almost totally deactivated) only reactions in the gas phase take place. Homogeneous reactions appear downstream of the monolith in the hot zone where temperatures are higher than the ignition temperature of *n*-decane (*i.e.* 208 °C). The residence time along the hot zone is 0.5 s which is one order of magnitude higher than the contact time through the monolith. The auto-ignition of *n*-decane provides enough energy to initiate the

reaction through homolytic fission of the alkane. Yet, *n*-decane pyrolysis investigations (*i.e.* without oxygen in the feed gas) at controlled temperatures (inside the second oven, *i.e.* activation oven, **Figure 1**), reveal a thermal cracking of hydrocarbons chains into shorter ones begins from 550 °C with a low yield into olefins (1.5 wt.%, **Figure 5**) despite a long residence time (0.5 s) throughout the reactor. Hence, olefins are rather released at this temperature from oxidative cracking than from thermal cracking.

Figure 6 displays the distribution of the olefins as a function of carbon chain length obtained in oxidative gas phase (aged catalyst) and on fresh catalyst. The olefins range from ethylene to double bond position of decene isomers. Therefore, the oxidative cracking implied in this homogeneous catalytic process is unselective. The olefins consist almost exclusively of linear α-olefins. Their distribution is asymmetrical towards light olefins in particular with increasing temperature. Schmidt *et al.* studied the oxidative cracking of *n*-decane on Pt or Rh alumina foam at temperatures beyond 700 °C [15,19,21]. They noted that the distribution of olefins flattens with decreasing temperature. This behavior was observed during pyrolysis tests (**Figure 5.B**) in which the distribution becomes even more asymmetrical toward light olefins with increasing temperature. Hence, high temperatures (> 600 °C) favor thermal multi-cracking and produces high yields into ethylene and propylene. The multi-cracking takes place as confirmed by the low 1-nonene/methane molar ratio (0.13). The lab scale millisecond reactor can process ~ 1.3 kg/day of *n*-decane and produce LAO up to 0.17 kg/day. It is obvious that after optimization and recycling, this technology can produce large amount of LAO autothermally even with long carbon chain length by using parallelized reactors.

Unlike pyrolysis (**Figure 5**), the oxidative cracking on fresh and aged catalyst (*i.e.* with and without heterogeneous reaction, **Figure 6**) yields all possible double bond positions of decene isomers (**Table 2**) including dec-1-ene which is the only isomer of industrial

importance. This indicates that their formation takes place in the gas phase and involves reaction with oxygenated species, namely O_2, $HO^{\bullet}$ [44,45].

The oxygenated products were identified by GC-MS and quantified by GC-FID. **Table 3** classifies the products into two families according to their carbon number: ketones, oxiranes and tetrahydrofurans with ten carbon atoms and the second ones to aldehydes with less than ten carbons. Ketones and cyclic ethers result from the decomposition of the decyl hydroperoxy radical through H atom transfer [44,46] while aldehydes are formed through β-scission [44,46]. This path which requires a C-C bond cleavage is more energetic. **Figure 7 and Figure 8** display the mass distribution of ketones, oxiranes, tetrahydrofurans (THF) and aldehydes according to the carbonyl position or the chain length of alkyls, while the distribution of aldehydes is a function of the carbon chain length. Despite a higher yield of oxygenated products formed in the gas phase (on aged catalyst), the proportion of the different families is identical to that obtained on the fresh catalyst in which homogeneous reactions also occur downstream of the catalyst. The main products are aldehydes and THF (about 40 % each), then oxirane (13-16 %) and ketones (8 %). Among the products resulting from hydrogen transfer without C-C bond cleavage, long chain alkanes mainly form THF as demonstrated by Dagaut *et al.* [44]. No decanal is observed which suggests that addition of O_2 only occurs on secondary carbons.

Oxygenated compounds formation involve two successive steps (**Figure 9**) (1) O_2 addition on secondary carbon and (2) H (primary and secondary) transfer no further away than 1,6. For example: for the 2-heptyl-3-methyloxirane, which corresponds to the oxirane 1,7 according to the **Figure 7** abscissa, the first step can occur on carbons in equivalent positions 2 and 9 or 3 and 8 of *n*-decane backbone. Two hydrogens are bonded on each of them and *n*-decane contains 16 secondary hydrogens. Therefore the probability of O_2 addition is 2/16 for each position, assuming a similar energy barrier for all secondary hydrogen abstraction at the

temperatures involved in OC [47]. If the peroxy radical is located on position 2 or 9, the H transfer 1,4 has to occur on hydrogens bonded on carbons in positions 3 or 8, respectively. Two hydrogens are bonded on each of these carbon atoms, and ten hydrogen atoms are at a distance of an H transfer 1,6. Therefore the probability for each pathway is $(\frac{2}{16}) \times (\frac{2}{10})$. Likewise, if the peroxy radical is located on positions 3 or 8 the H transfer 1,4 has to occur on hydrogens bonded on carbons in positions 2 or 9 respectively. Therefore the probability for each pathway is $(\frac{2}{16}) \times (\frac{2}{12})$. The 2-heptyl-3-methyloxirane formation probability is, considering the absence of steric hindrance effects for each mechanistic steps: $(\frac{2}{16}) \times (\frac{2}{10} + \frac{2}{10} + \frac{2}{12} + \frac{2}{12})$. Distributions are calculated from the normalization of the probabilities inside the considered family ($\text{Distribution} = \frac{\text{Probability}}{\sum \text{Probabilities}}$) and the calculated yields result from multiplying calculated distributions with experimental yield of the considered family (*i. e.* ketones, oxiranes, tetrahydrofurans or aldehydes). The probabilities for other oxygenated compounds are depicted in **Table SI. 2**. The yields into oxygenated products, except aldehydes, fits with those calculated only from the statistical distribution of hydrogen on the *n*-decane backbone (**Figure 7** and **9**). This particular distribution indicates a strong quenching that impedes secondary reactions.

Figure 9 summarizes the main mechanisms involved in the *n*-decane oxidative cracking. A few amount of the reactant is oxidized into CO and CO_2 on the metal catalyst, releasing heat, producing hydrogen subsequently to WGSR as well as free radicals which further initiate homogeneous reactions downstream of the catalyst. In the gas phase, the initial step is an unselective H-atom abstraction yielding to an alkyl radical ($R^{\bullet}$). Yet, without oxygen (pyrolysis condition), $R^{\bullet}$ cracks through β-scission into light olefins and a shorter alkyl radical which can release another hydrogen atom leading to olefin or further cracks into light olefins. Under oxidative condition, the alkyl radicals directly add molecular oxygen to

produce the alkylperoxy radical ($ROO^{\bullet}$), an important intermediate which can either rearrange into decenes, or following different H-transfers, to ketones, oxiranes and tetrahydrofurans or to aldehyde and α-olefins (desired products) through β-C scission.

4. Conclusion

The "millisecond" cracking process is an alternative to the conventional homogeneous process for the production of α-olefins. The oxidative cracking, contrariwise to catalytic and steam cracking processes, allows obtaining long chain α-linear olefins through an auto-thermal route. This process combines heterogeneous and homogeneous chemistry leading to non-equilibrium species. Exothermic catalytic and homogeneous reactions supply the heat for the initiation of radical reactions leading to the desired products in the gas phase. α-olefins and oxygenated products are formed concomitantly through a radical mechanism involving molecular oxygen and result from the decomposition of decylperoxy radicals intermediates. Above the *n*-decane thermal cracking temperature, millisecond reactor switched to light olefins production. Therefore, the development of this technology for LAO synthesis requires to consider thermal and chemical phenomena that are mutually related and a fine control of gas phase temperature is necessary *e.g.* through reactor engineering or combustion catalyst development.

Very short contact times and oxygenated function stability settled in this oxidative cracking process could be applied in bio-refinery on oleic acid to produce di α-olefinic compounds and α-olefinic acids, which are very high valuable biosourced products.

Credit author statement

Hugo Cruchade: Investigation, Writing- Original draft preparation. **Claude Veit:** Resources. **Jean-Jacques Colin:** Resources. **Romain Beauchet:** Methodology. **Yann Batonneau:** Writing- Reviewing and Editing. **Yannick Pouilloux:** Conceptualization.

Bertrand Leroux: Methodology. **Ludovic Pinard:** Conceptualization, Writing- Reviewing and Editing, Visualization.

Acknowledgment

The authors acknowledge financial supports from the European Union (ERDF), "Région Nouvelle Aquitaine". Hugo Cruchade thanks "Ministère de l'enseignement supérieur, de la recherche et de l'innovation" for Ph.D. grant.

References

[1] G.R. Lappin, L.H. Nemec, J.D. Sauer, J.D. Wagner, Olefins, Higher, in: Kirk-Othmer Encycl. Chem. Technol., American Cancer Society, 2010: pp. 1–20.

[2] K. Weissermel, H.-J. Arpe, Industrial organic chemistry, 3rd completely rev. ed, VCH, Weinheim ; New York, 1997.

[3] A. Forestière, H. Olivier-Bourbigou, L. Saussine, Oligomerization of Monoolefins by Homogeneous Catalysts, Oil Gas Sci. Technol. - Rev. IFP. 64 (2009) 649–667. https://doi.org/10.2516/ogst/2009027.

[4] W. Keim, Oligomerization of Ethylene to α-Olefins: Discovery and Development of the Shell Higher Olefin Process (SHOP), Angew. Chem. Int. Ed. 52 (2013) 12492–12496. https://doi.org/10.1002/anie.201305308.

[5] A.S. Bodke, S.S. Bharadwaj, L.D. Schmidt, The Effect of Ceramic Supports on Partial Oxidation of Hydrocarbons over Noble Metal Coated Monoliths, J. Catal. 179 (1998) 138–149. https://doi.org/10.1006/jcat.1998.2224.

[6] D.A. Hickman, L.D. Schmidt, Synthesis Gas Formation by Direct Oxidation of Methane over Monoliths, in: S.T. Oyama, J.W. Hightower (Eds.), Catal. Sel. Oxid., American

Chemical Society, Washington, DC, 1993: pp. 416–426. https://doi.org/10.1021/bk-1993-0523.ch032.

[7] R. Horn, K. Williams, N. Degenstein, A. Bitschlarsen, D. Dallenogare, S. Tupy, L.D. Schmidt, Methane catalytic partial oxidation on autothermal Rh and Pt foam catalysts: Oxidation and reforming zones, transport effects, and approach to thermodynamic equilibrium, J. Catal. 249 (2007) 380–393. https://doi.org/10.1016/j.jcat.2007.05.011.

[8] P. Torniainen, X. Chu, L. Schmidt, Comparison of monolith-supported metals for the direct oxidation of methane to syngas1, J. Catal. 146 (1994) 1–10. https://doi.org/10.1016/0021-9517(94)90002-7.

[9] D.A. Hickman, L.D. Schmidt, Production of Syngas by Direct Catalytic Oxidation of Methane, Science. 259 (1993) 343–346. https://doi.org/10.1126/science.259.5093.343.

[10] M. Huff, P.M. Torniainen, D.A. Hickman, L.D. Schmidt, Partial Oxidation of CH4, C2H6, and C3H8 on Monoliths at Short Contact Times, in: H.E. Curry-Hyde, R.F. Howe (Eds.), Stud. Surf. Sci. Catal., Elsevier, 1994: pp. 315–320. https://doi.org/10.1016/S0167-2991(08)63887-2.

[11] M. Huff, P.M. Torniainen, L.D. Schmidt, Partial oxidation of alkanes over noble metal coated monoliths, Catal. Today. 21 (1994) 113–128. https://doi.org/10.1016/0920-5861(94)80038-3.

[12] M. Huff, L.D. Schmidt, Ethylene formation by oxidative dehydrogenation of ethane over monoliths at very short contact times, J. Phys. Chem. 97 (1993) 11815–11822. https://doi.org/10.1021/j100147a040.

[13] B.C. Michael, D.N. Nare, L.D. Schmidt, Catalytic partial oxidation of ethane to ethylene and syngas over Rh and Pt coated monoliths: Spatial profiles of temperature and composition, Chem. Eng. Sci. 65 (2010) 3893–3902. https://doi.org/10.1016/j.ces.2010.03.033.

[14] M. Huff, L.D. Schmidt, Production of Olefins by Oxidative Dehydrogenation of Propane and Butane over Monoliths at Short Contact Times, J. Catal. 149 (1994) 127–141. https://doi.org/10.1006/jcat.1994.1278.

[15] G.J. Panuccio, B.J. Dreyer, L.D. Schmidt, A comparison of the catalytic partial oxidation of C1 to C16 normal paraffins, AIChE J. 53 (2007) 187–195. https://doi.org/10.1002/aic.11057.

[16] A.G. Dietz, A.F. Carlsson, L.D. Schmidt, Partial Oxidation of C5 and C6 Alkanes over Monolith Catalysts at Short Contact Times, J. Catal. 176 (1998) 459–473. https://doi.org/10.1006/jcat.1998.2065.

[17] G.J. Panuccio, K.A. Williams, L.D. Schmidt, Contributions of heterogeneous and homogeneous chemistry in the catalytic partial oxidation of octane isomers and mixtures on rhodium coated foams, Chem. Eng. Sci. 61 (2006) 4207–4219. https://doi.org/10.1016/j.ces.2006.02.010.

[18] R.P. O'connor, E.J. Klein, L.D. Schmidt, High yields of synthesis gas by millisecond partial oxidation of higher hydrocarbons, Catal. Lett. 70 (2000) 99–107.

[19] J. Krummenacher, High yields of olefins and hydrogen from decane in short contact time reactors: rhodium versus platinum, J. Catal. 222 (2004) 429–438. https://doi.org/10.1016/j.jcat.2003.12.005.

[20] N. Degenstein, R. Subramanian, L. Schmidt, Partial oxidation of n-hexadecane at short contact times: Catalyst and washcoat loading and catalyst morphology, Appl. Catal. Gen. 305 (2006) 146–159. https://doi.org/10.1016/j.apcata.2006.02.060.

[21] J.J. Krummenacher, K.N. West, L.D. Schmidt, Catalytic partial oxidation of higher hydrocarbons at millisecond contact times: decane, hexadecane, and diesel fuel, J. Catal. 215 (2003) 332–343. https://doi.org/10.1016/S0021-9517(03)00011-3.

[22] D.A. Hickman, E.A. Haupfear, L.D. Schmidt, Synthesis gas formation by direct oxidation of methane over Rh monoliths, Catal. Lett. 17 (1993) 223–237. https://doi.org/10.1007/BF00766145.

[23] S.S. Bharadwaj, L.D. Schmidt, Catalytic partial oxidation of natural gas to syngas, Fuel Process. Technol. 42 (1995) 109–127. https://doi.org/10.1016/0378-3820(94)00098-E.

[24] A. Bodke, D. Henning, L.D. Schmidt, A comparison of H 2 addition to 3 ms partial oxidation reactions, Catal. Today. 61 (2000) 65–72.

[25] F.D.T. Caputo, G. Russo, A. Di Benedetto, R. Pirone, Modeling ethane oxy-dehydrogenation over monolithic combustion catalysts, AIChE J. 50 (2004) 2233–2245. https://doi.org/10.1002/aic.10180.

[26] A. Beretta, P. Forzatti, High-Temperature and Short-Contact-Time Oxidative Dehydrogenation of Ethane in the Presence of Pt/Al2O3 and BaMnAl11O19 Catalysts, J. Catal. 200 (2001) 45–58. https://doi.org/10.1006/jcat.2001.3192.

[27] G. Panuccio, L. Schmidt, Increasing olefins by H2 and CH4 addition to the catalytic partial oxidation of n-octane, Appl. Catal. Gen. 313 (2006) 63–73. https://doi.org/10.1016/j.apcata.2006.07.011.

[28] L.D. Schmidt, Millisecond chemical reactions and reactors, in: Stud. Surf. Sci. Catal., Elsevier, 2000: pp. 61–81. https://doi.org/10.1016/S0167-2991(00)80945-3.

[29] F. Donsì, K.A. Williams, L.D. Schmidt, A Multistep Surface Mechanism for Ethane Oxidative Dehydrogenation on Pt- and Pt/Sn-Coated Monoliths, Ind. Eng. Chem. Res. 44 (2005) 3453–3470. https://doi.org/10.1021/ie0493356.

[30] A. Beretta, P. Forzatti, E. Ranzi, Production of Olefins via Oxidative Dehydrogenation of Propane in Autothermal Conditions, J. Catal. 184 (1999) 469–478. https://doi.org/10.1006/jcat.1999.2447.

[31] M.C. Huff, I.P. Androulakis, J.H. Sinfelt, S.C. Reyes, The Contribution of Gas-Phase Reactions in the Pt-Catalyzed Conversion of Ethane–Oxygen Mixtures, J. Catal. 191 (2000) 46–54. https://doi.org/10.1006/jcat.1999.2798.

[32] D. A. Henning, L. D. Schmidt, Oxidative dehydrogenation of ethane at short contact times: species and temperature profiles within and after the catalyst, Chem. Eng. Sci. 57 (2002) 2615–2625. https://doi.org/10.1016/S0009-2509(02)00155-0.

[33] R. Horn, N.J. Degenstein, K.A. Williams, L.D. Schmidt, Spatial and temporal profiles in millisecond partial oxidation processes, Catal. Lett. 110 (2006) 169–178. https://doi.org/10.1007/s10562-006-0117-8.

[34] E. Ranzi, T. Faravelli, P. Gaffuri, E. Garavaglia, A. Goldaniga, Primary Pyrolysis and Oxidation Reactions of Linear and Branched Alkanes, Ind. Eng. Chem. Res. 36 (1997) 3336–3344. https://doi.org/10.1021/ie960603c.

[35] S.W. Benson, III - Bond energies, J. Chem. Educ. 42 (1965) 502. https://doi.org/10.1021/ed042p502.

[36] D. Amariei, R. Amrousse, Y. Batonneau, R. Brahmi, C. Kappenstein, B. Cartoixa, Monolithic catalysts for the decomposition of energetic compounds, in: Stud. Surf. Sci. Catal., Elsevier, 2010: pp. 35–42. https://doi.org/10.1016/S0167-2991(10)75005-9.

[37] J.T. Scanlon, D.E. Willis, Calculation of Flame Ionization Detector Relative Response Factors Using the Effective Carbon Number Concept, J. Chromatogr. Sci. 23 (1985) 333–340. https://doi.org/10.1093/chromsci/23.8.333.

[38] T. Ren, M. Patel, K. Blok, Olefins from conventional and heavy feedstocks: Energy use in steam cracking and alternative processes, Energy. 31 (2006) 425–451. https://doi.org/10.1016/j.energy.2005.04.001.

[39] G.J. Panuccio, L.D. Schmidt, Species and temperature profiles in a differential sphere bed reactor for the catalytic partial oxidation of n-octane, Appl. Catal. Gen. 332 (2007) 171–182. https://doi.org/10.1016/j.apcata.2007.06.035.

[40] L.D. Schmidt, O. Deutschmann, C.T. Goralski, Modeling the Partial Oxidation of Methane to Syngas at Millisecond Contact Times, in: Stud. Surf. Sci. Catal., Elsevier, 1998: pp. 685–692. https://doi.org/10.1016/S0167-2991(98)80511-9.

[41] R.P. O'Connor, E.J. Klein, D. Henning, L.D. Schmidt, Tuning millisecond chemical reactors for the catalytic partial oxidation of cyclohexane, Appl. Catal. Gen. 238 (2003) 29–40. https://doi.org/10.1016/S0926-860X(02)00100-X.

[42] R.P. O'Connor, L.D. Schmidt, O. Deutschmann, Simulating cyclohexane millisecond oxidation: Coupled chemistry and fluid dynamics, AIChE J. 48 (2002) 1241–1256. https://doi.org/10.1002/aic.690480611.

[43] D.I. Iordanoglou, A.S. Bodke, L.D. Schmidt, Oxygenates and Olefins from Alkanes in a Single-Gauze Reactor at Short Contact Times, J. Catal. 187 (1999) 400–409. https://doi.org/10.1006/jcat.1999.2637.

[44] P. Dagaut, M. Reuillon, M. Cathonnet, D. Voisin, High pressure oxidation of normal decane and kerosene in dilute conditions from low to high temperature, J. Chim. Phys. 92 (1995) 47–76. https://doi.org/10.1051/jcp/1995920047.

[45] C.F. Cullis, M.M. Hirschler, R.L. Rogers, The Oxidation of Decane in the Liquid and Gaseous Phases, Proc. R. Soc. Math. Phys. Eng. Sci. 375 (1981) 543–563. https://doi.org/10.1098/rspa.1981.0067.

[46] R.G. Compton, C.H. Bamford, C.F.H. Tipper†, Gas Phase Combustion, Elsevier, 1977.

[47] K.C. Hunter, A.L.L. East, Properties of C–C Bonds in n-Alkanes: Relevance to Cracking Mechanisms, J. Phys. Chem. A. 106 (2002) 1346–1356. https://doi.org/10.1021/jp0129030.

[48] W.K. Hall, B.E. Spiewak, R.D. Cortright, J.A. Dumesic, H. Knözinger, H. Pfeifer, V.B. Kazansky, G.C. Bond, Characterization of Solid Catalysts, in: Handb. Heterog. Catal., John Wiley & Sons, Ltd, 2008: pp. 689–770.

Figure caption list

Figure 1. Flowsheet of the millisecond reactor rig.

Figure 2. Temperatures measured at 0 (red), 10 (black) and 55 mm (grey) downstream of the outlet cross-section of the monolith as a function of time-on-stream on fresh and aged catalysts at $\Phi = 5$, then without *n*-decane. Dashed lines: reactor cooling (air) without reaction.

Figure 3. Product yields and oxygen conversion (■) on the fresh and aged catalysts at different time-on-stream (and related equilibrium catalyst temperatures) and during the blank test at a time-on-stream of 100 min (and related equilibrium gas phase temperature).

Figure 4. H_2 yield on the fresh and aged catalysts at different time-on-stream.

Figure 5. *n*-decane thermal cracking evaluation. (**A**) Conversion as a function of pyrolysis temperature and (**B**) olefins yields as a function of carbon chain length at 450, 550, 650 and 680 °C.

Figure 6. Bar chart of the yields into α-olefins (solid bars) and decenes isomers (gridded bar) as a function of carbon chain length obtained at different times on fresh (10 and 180 min) and aged catalysts (5 and 100 min).

Figure 7. Bar chart of the experimental yields and calculated distributions (■) into 10-carbons oxygenated compounds resulting from O_2 addition followed by hydrogen transfer (HT) obtained on fresh and aged catalysts after 180 and 100 min, respectively.

Figure 8. Bar chart of the experimental yields and calculated distributions (■) into aldehydes resulting from O_2 addition followed by hydrogen transfer (HT) obtained on fresh and aged catalysts after 180 and 100 min, respectively.

Figure 9. Mechanisms of carbonaceous products formation from *n*-decane oxidative cracking. In brackets: molar selectivities (fresh catalyst after 180 min (bold)/aged catalyst after 100 min).

Table caption list

Table 1. Physicochemical properties of the fresh and aged washcoated monolith catalysts.

Table 2. Products identified using GC-MS sorted and ranked by chemical function

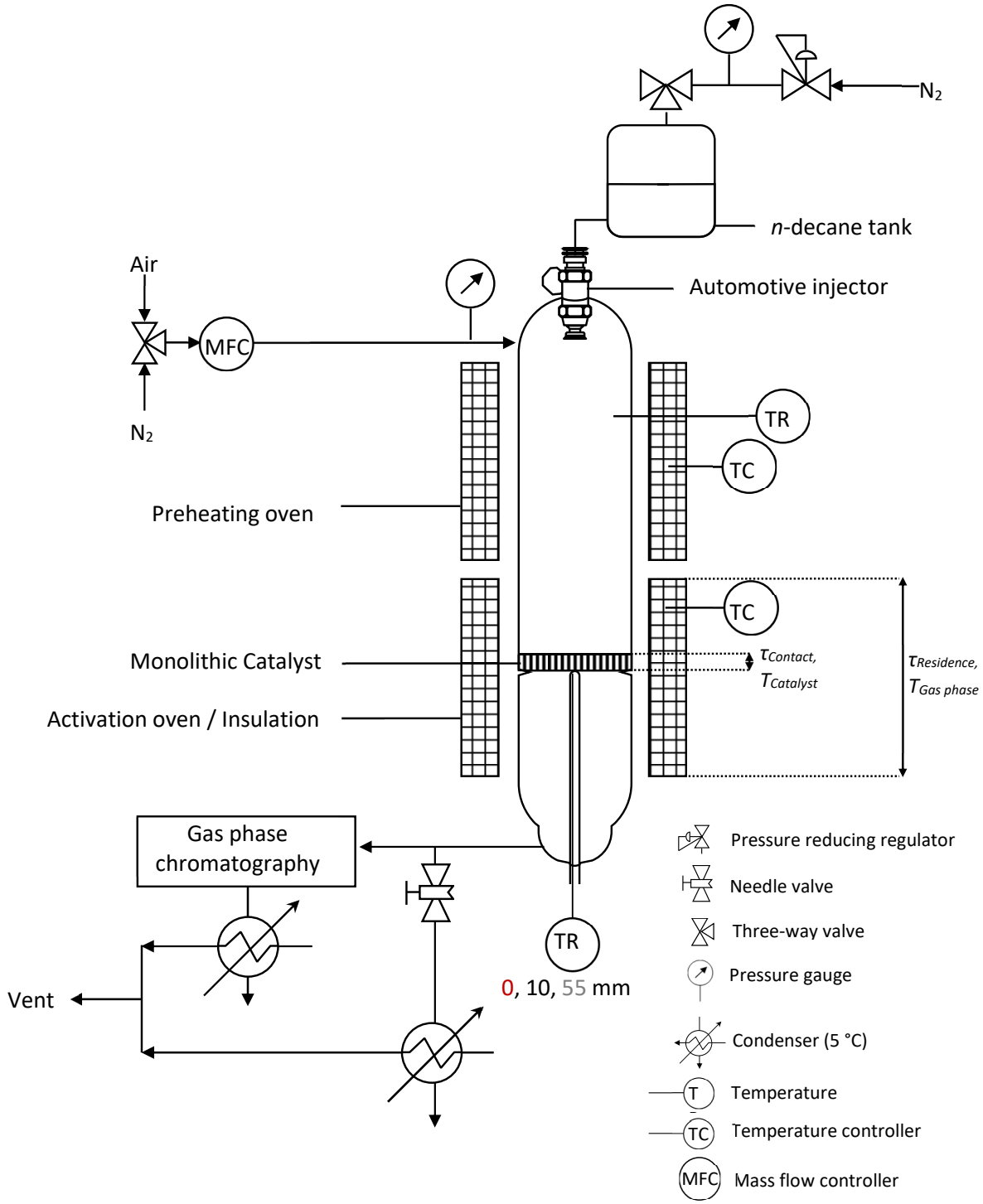

Figure 1. Flowsheet of the millisecond reactor rig.

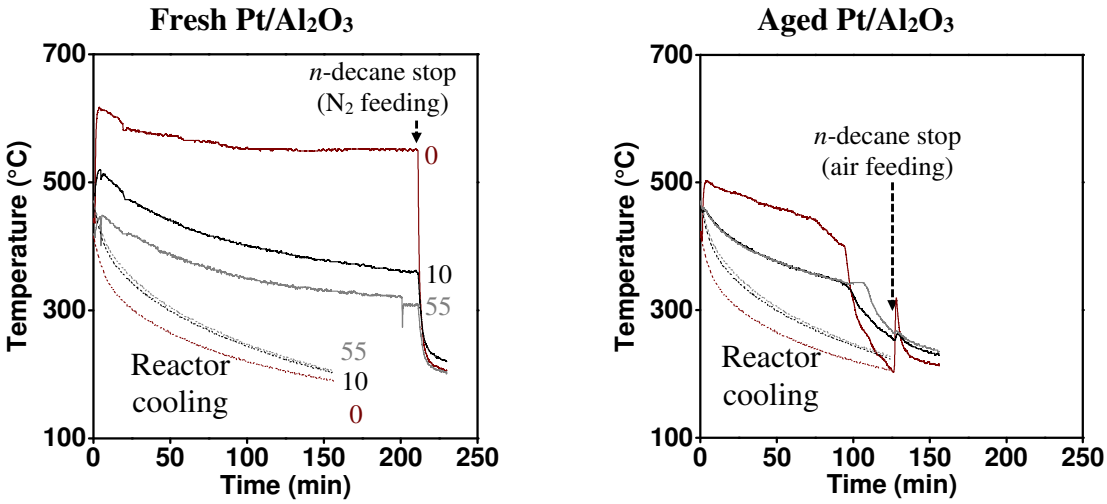

Figure 2. Temperatures measured at 0 (red), 10 (black) and 55 mm (grey) downstream of the outlet cross-section of the monolith as a function of time-on-stream on fresh and aged catalysts at Φ = 5, then without *n*-decane. Dashed lines: reactor cooling (air) without reaction.

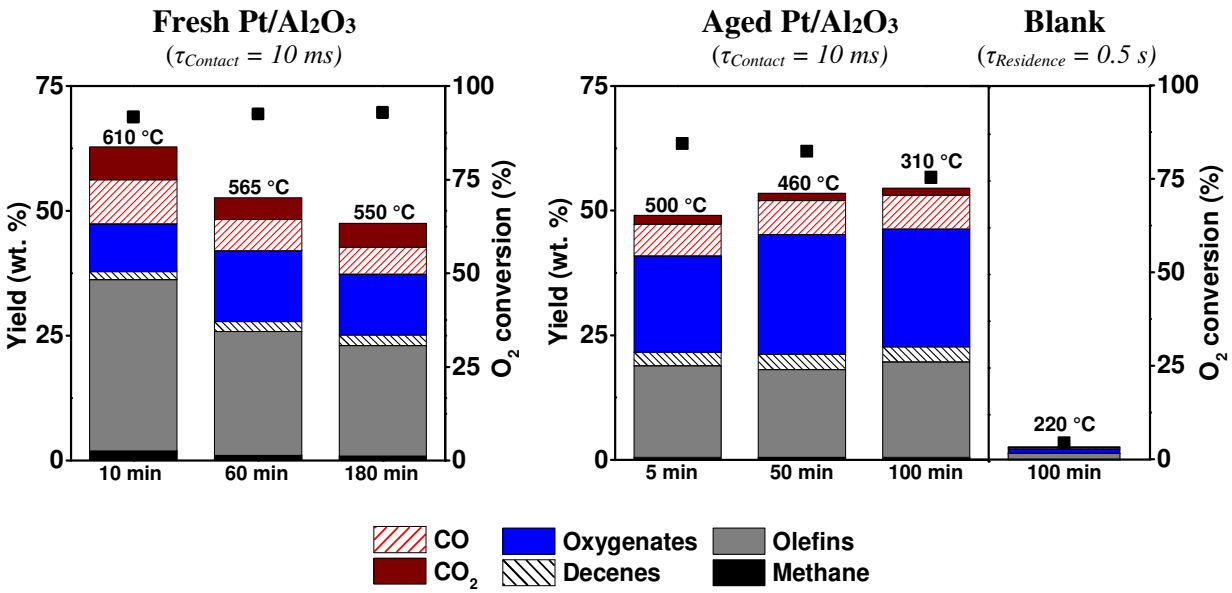

Figure 3. Product yields and oxygen conversion (■) on the fresh and aged catalysts at different time-on-stream (and related equilibrium catalyst temperatures) and during the blank test at a time-on-stream of 100 min (and related equilibrium gas phase temperature).

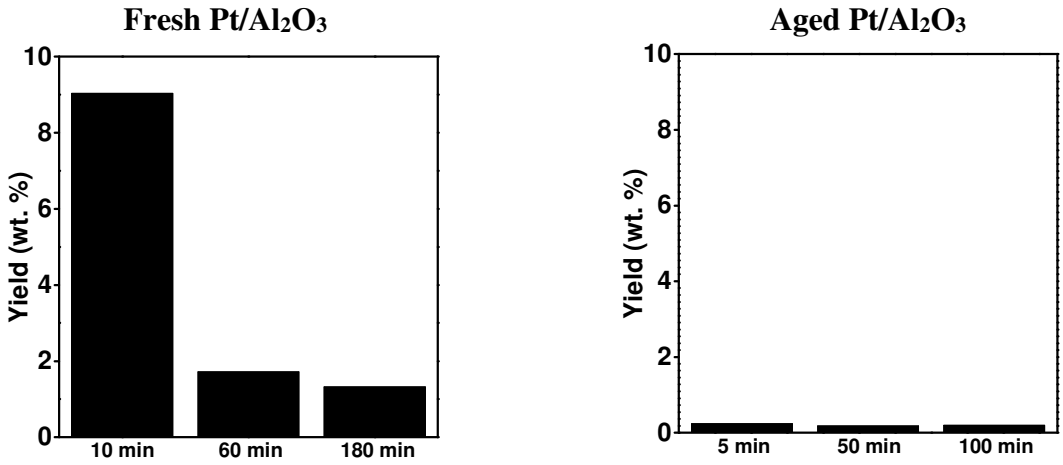

Figure 4. H_2 yield on the fresh and aged catalysts at different time-on-stream.

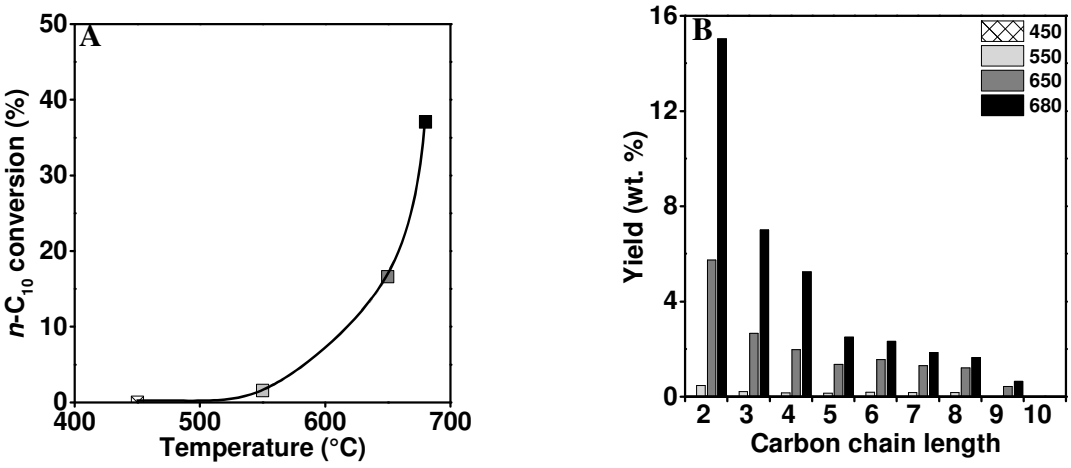

Figure 5. *n*-decane thermal cracking evaluation. (**A**) Conversion as a function of pyrolysis temperature and (**B**) olefins yields as a function of carbon chain length at 450, 550, 650 and 680 °C.

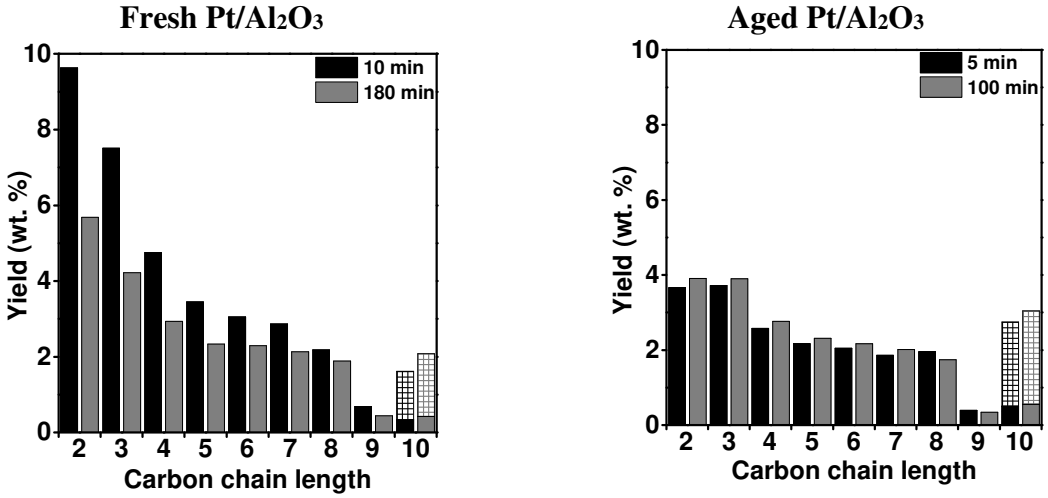

Figure 6. Bar chart of the yields into α-olefins (solid bars) and decenes isomers (gridded bar) as a function of carbon chain length obtained at different times on fresh (10 and 180 min) and aged catalysts (5 and 100 min).

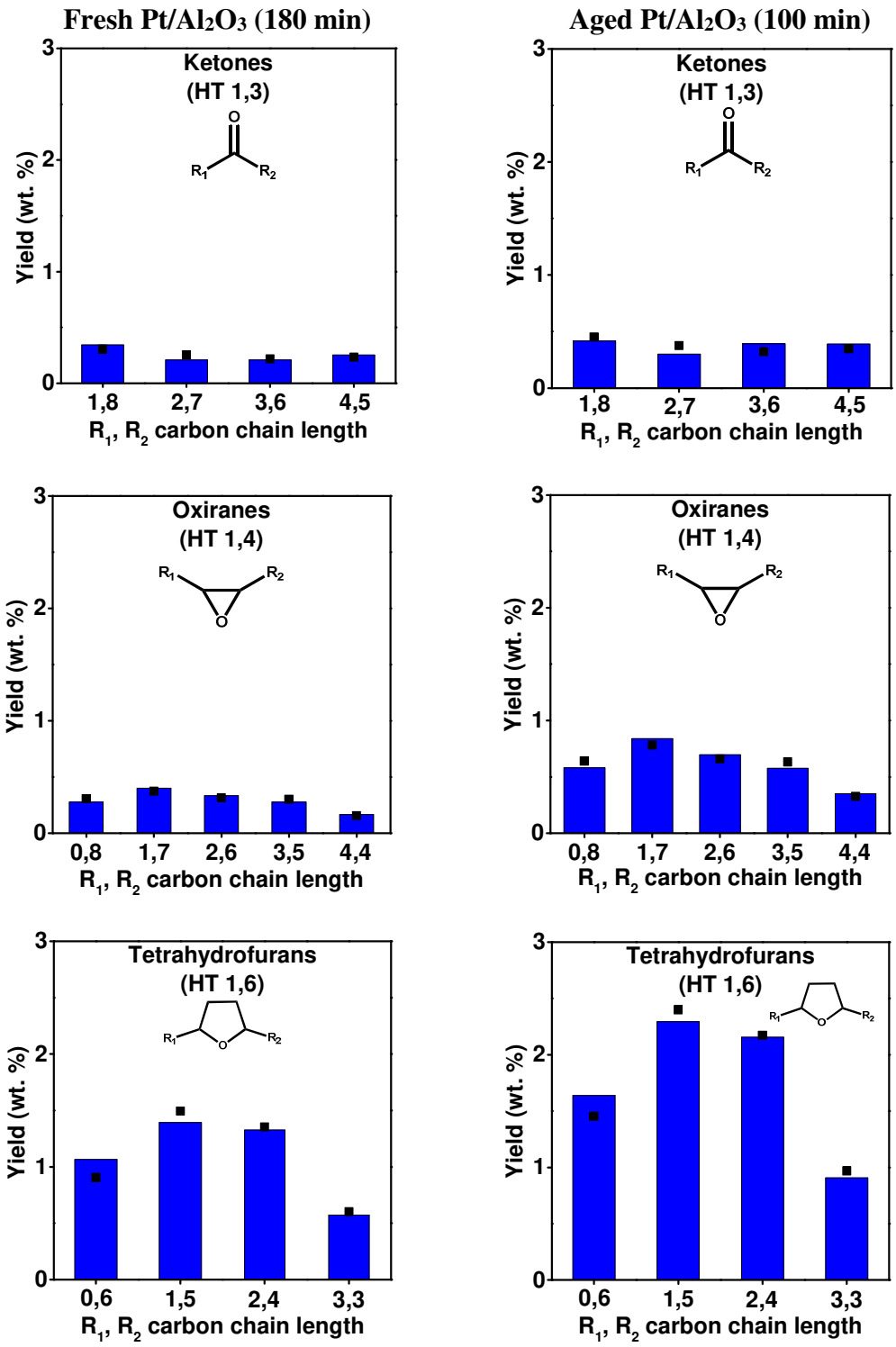

Figure 7. Bar chart of the experimental yields and calculated distributions (■) into 10-carbons oxygenated compounds resulting from O_2 addition followed by hydrogen transfer (HT) obtained on fresh and aged catalysts after 180 and 100 min, respectively.

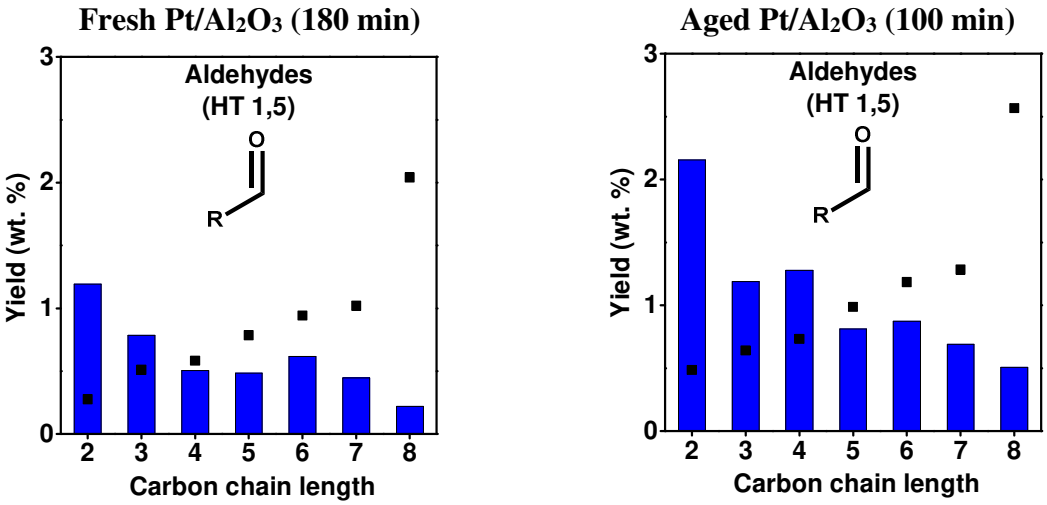

Figure 8. Bar chart of the experimental yields and calculated distributions (■) into aldehydes resulting from O_2 addition followed by hydrogen transfer (HT) obtained on fresh and aged catalysts after 180 and 100 min, respectively.

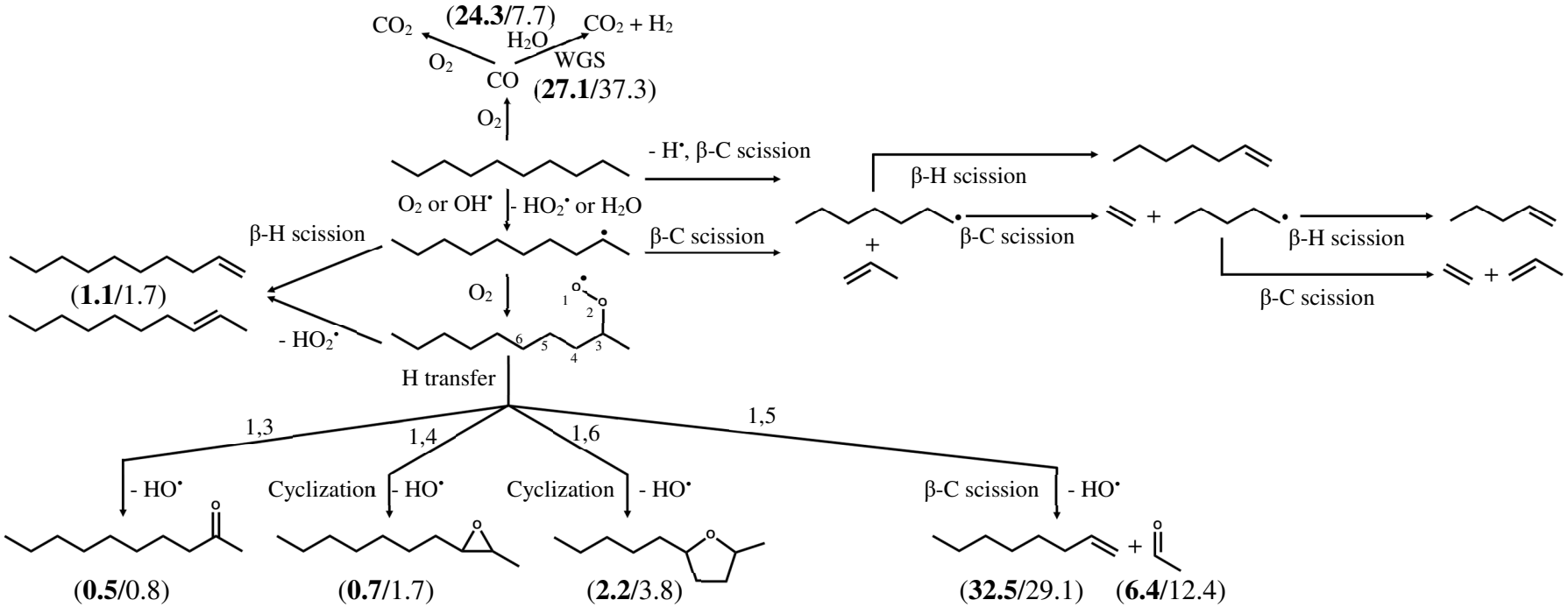

Figure 9. Mechanisms of carbonaceous products formation from *n*-decane oxidative cracking. In brackets: molar selectivities (fresh catalyst after 180 min (bold)/aged catalyst after 100 min).

Table 1. Physicochemical properties of the fresh and aged washcoated monolith catalysts.

	Al_2O_3 [1]	V_{meso} [2]	S_{BET} [2]	Pt [3]	$\bar{d}_{Pt}$ [4]	D [5]	A_0 [6]
	wt.%	/ $cm^3\ g^{-1}$ ($cm^3\ g_{washcoat}^{-1}$)	/ $m^2\ g_{tot}^{-1}$ ($m^2\ g_{washcoat}^{-1}$)	mol.%	/ nm	%	/ mol $h^{-1}\ g_{Pt}^{-1}$
Cordierite	/	0	0	/	/	/	/
Fresh	9.8	0.02 (0.20)	13.2 (144.0)	0.7	1.4	81	11.9
(Before aging)	10.1	0.02 (0.18)	13.8 (150.7)	1.3	1.5	77	n.d.[7]
Aged	n.d.[7]	0.01 (n.d.[7])	3.8 (n.d.[7])	0.8	11.1	10	5.6

1 Washcoat content of the impregnated catalyst as measured by gravimetry, 2 external surface and micropore volume calculated using the t-plot method, 3 measured by ICP $\%Pt = n_{Pt}/(n_{Pt}+n_{Al2O3})$, 4 measured by TEM, 5 dispersion (D) calculated from $\bar{d}_{Pt}$ and the equation in [48], 6 propane dehydrogenation initial activity and 7 not determined.

Table 2. Products identified using GC-MS sorted and ranked by chemical function

Carbon chain length	Molecule	Skeletal formula	B_p*-(T_{AI})** /°C
10	dec-1-ene	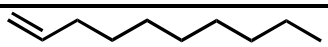	171-(235)
	dec-2-ene	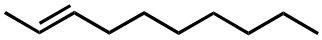	174 (Z) 173 (E)
	dec-3-ene	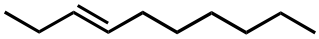	171(Z) 171 (E)
	dec-4-ene	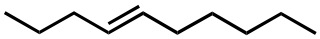	171 (Z) 171 (E)
	dec-5-ene		171 (Z) 170 (E)
10	decan-2-one	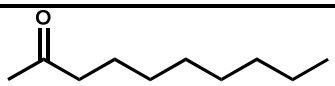	210
	decan-3-one	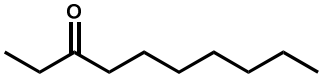	203
	decan-4-one	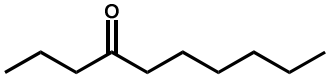	206
	decan-5-one	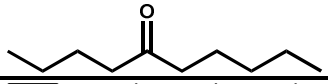	204
10	2-octyloxirane	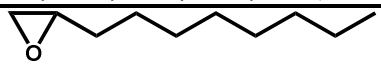	/
	2-heptyl-3-methyloxirane	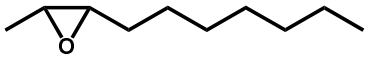	
	2-ethyl-3-hexyloxirane	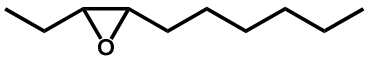	
	2-pentyl-3-propyloxirane		
	2,3-dibutyloxirane		
10	2-hexyltetrahydrofuran	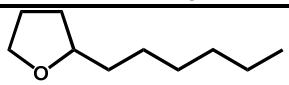	/
	2-methyl-5-pentyltetrahydrofuran	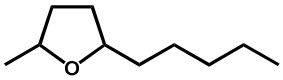	
	2-butyl-5-ethyltetrahydrofuran	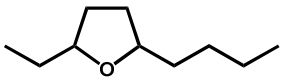	
	2,5-dipropyltetrahydrofuran	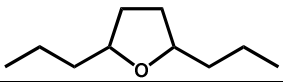	
2	Ethanal		20-(185)
3	Propanal		48-(207)
4	Butanal	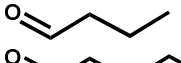	75-(230)
5	Pentanal	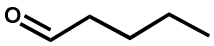	103-(222)
6	Hexanal	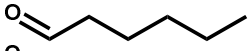	128
7	Heptanal	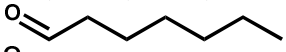	153
8	Octanal		174

*Boiling point, **Autoignition temperature

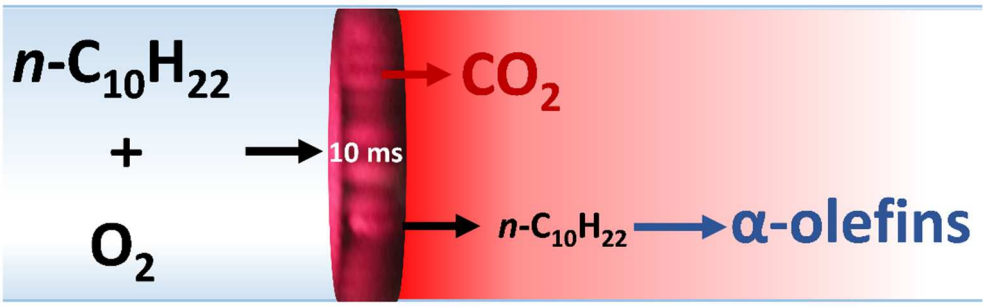
n-C10H22
+
O2
10 ms
CO2
n-C10H22
α-olefins